




Cryo-Fluorescence Tomography as a Tool for Visualizing Whole-Body Inflammation Using Perfluorocarbon Nanoemulsion Tracers

Benjamin I. Leach¹ · Deanne Lister² · Stephen R. Adams³ · Julie Bykowski¹ · Amy B. Schwartz¹ · Patrick McConville² · Hemi Dimant² · Eric T. Ahrens¹ 

Received: 30 October 2023 / Revised: 30 May 2024 / Accepted: 3 June 2024
© The Author(s), under exclusive licence to World Molecular Imaging Society 2024

Abstract

Purpose We explore the use of intravenously delivered fluorescent perfluorocarbon (PFC) nanoemulsion tracers and multi-spectral cryo-fluorescence tomography (CFT) for whole-body tracer imaging in murine inflammation models. CFT is an emerging technique that provides high-resolution, three-dimensional mapping of probe localization in intact animals and tissue samples, enabling unbiased validation of probe biodistribution and minimizes reliance on laborious histological methods employing discrete tissue panels, where disseminated populations of PFC-labeled cells may be overlooked. This methodology can be used to streamline the development of new generations of non-invasive, cellular-molecular imaging probes for *in vivo* imaging.

Procedures Mixtures of nanoemulsions with different fluorescent emission wavelengths were administered intravenously to naïve mice and models of acute inflammation, colitis, and solid tumor. Mice were euthanized 24 h post-injection, frozen en bloc, and imaged at high resolution (~50 µm voxels) using CFT at multiple wavelengths.

Results PFC nanoemulsions were visualized using CFT within tissues of the reticuloendothelial system and inflammatory lesions, consistent with immune cell (macrophage) labeling, as previously reported in *in vivo* magnetic resonance and nuclear imaging studies. The CFT signals show pronounced differences among fluorescence wavelengths and tissues, presumably due to autofluorescence, differential fluorescence quenching, and scattering of incident and emitted light.

Conclusions CFT is an effective and complementary methodology to *in vivo* imaging for validating PFC nanoemulsion biodistribution at high spatial localization, bridging the resolution gap between *in vivo* imaging and histology.

Keywords Cryo-fluorescence tomography · Cancer · Perfluorocarbon · Nanoemulsion · Fluorine-19 · MRI · PET · Macrophage · Inflammation · Mouse

Introduction

Non-invasive imaging techniques have been an important tool for diagnosis and stratification of inflammation, both clinically and in animal models. Immune cell probes developed for *in vivo* imaging modalities such as positron emission tomography (PET) and magnetic

resonance imaging (MRI) enable temporal visualizations of immune cell dynamics and inflammatory processes [1]. The evaluation of new *in vivo* molecular imaging markers requires same-subject signal validation via high-resolution histological methods in tissue slices and assays of necropsied tissues, for example by flow cytometry of single cell suspensions, to confirm target specificity. When comparing whole-body *in vivo* image data to histological/single cell assays, there remains a ‘resolution gap’ of ~10 to 1,000 µm in the ability to visualize and validate labeling of inflammatory immune cells. Additionally, localized populations of immune cells and small dispersed lesion sites may not be adequately sampled in representative histology and cell assay tissue panels. To address these challenges, we explore the use of cryo-fluorescence tomography (CFT),

✉ Eric T. Ahrens
etanosam@gmail.com

¹ Department of Radiology, University of California, San Diego, La Jolla, CA 92093, USA

² Invicro LLC, Needham, MA 02494, USA

³ Department of Pharmacology, University of California, San Diego, La Jolla, CA 92093, USA

a three-dimensional histology technique [2–4] pioneered by Wilson and coworkers [2], in which the entire animal or intact organ/tissue is mounted in optimal cutting temperature (OCT) cryo-embedding compound *en bloc* and sectioned robotically using a modified cryo-macrotome in 50–100 μm slices. White-light and multi-spectral fluorescence images are acquired after each cut using a camera positioned over the block, and these data are reconstructed into high-resolution three-dimensional (3D) images. CFT has the ability to provide whole animal 3D images at an intermediate-to-high resolution, bridging the resolution gap between *in vivo* imaging and histology.

Perfluorocarbon (PFC) nanoemulsion tracer probes are a versatile platform for labeling immune cells, including inflammatory macrophages. Nanoemulsions can be used to label cells in culture *ex vivo* or via '*in situ*' labeling, where the agent is administered intravenously and nanoemulsion droplets are endocytosed by phagocytic immune cells like macrophages at sites of inflammation [5–7]. Nanoemulsions are formulated via emulsification of PFC into an aqueous colloidal suspension, commonly employing phospholipids or synthetic polymers as a surfactant for stabilization [8], to yield small, uniform droplets (typically 100–200 nm in diameter). A variety of moieties may be chemically incorporated into liquid-core PFC probes, enabling sensitive *in vivo* molecular imaging by ^{19}F MRI [9], PET [10], and fluorescence imaging [11, 12] via chemical attachment to the surfactant, or through conjugation to fluororous substituents that partition into the PFC oil [12, 13]. These 'dual-mode' fluorescent PFC nanoemulsions have proven to be excellent cell labels for optical detection due to their bright fluorescence, low toxicity, and long retention time in viable cells [12]. PFCs are lipophobic, hydrophobic, do not incorporate into cell membranes [14], and are not degraded by enzymes or in low pH environments. They have been rigorously tested for biological safety with no observed adverse effects on cell viability or function [15].

In this preliminary study, we investigate the combined use of PFC nanoemulsions with CFT to evaluate whole-body visualization of probe biodistribution. We perform high-resolution CFT in murine models of acute inflammation, inflammatory bowel disease (IBD), and solid tumor-associated macrophages (TAMs), where prior *in vivo* ^{19}F MRI and ^{89}Zr PET studies have been performed using functionalized PFC nanoemulsions [10]. We also explore the apparent nanoemulsion detectability across tissues using fluorescent dyes with different emission/absorption wavelengths, and in the context of intrinsic tissue autofluorescence.

Methods

PFC Nanoemulsions

Nanoemulsions were commercially obtained (Celsense, Pittsburgh, PA) and are comprised of emulsified perfluoropolyether (PFPE) oil with ~ 180 nm mean droplet size, suitable for direct intravenous injection. Each manufacturer-supplied nanoemulsion contained fluorophores of different wavelengths: Texas Red (ex/em 589/615 nm; V-sense 1000 DM-Red), green (fluorescein, FITC, ex/em 419/512 nm; V-Sense 1000 DM-Green), or near-infrared (NIR, Cy7, ex/em 756/779 nm; V-sense 1000 DM-NIR). Fluorescent nanoemulsions were prepared for injection as indicated below, using either 200 μl of a single color emulsion or equal proportions by volume of multiple emulsions (100 μl per color) to generate di- or tri-colored cocktails (200 or 300 μl total volume, respectively).

Control Mice

All animal experiments were performed in accordance with the guidelines provided by the UC San Diego Institutional Animal Care and Use Committee (IACUC) and the National Institute of Health Guide for the Care and Use of Laboratory Animals. Wild-type C57BL/6 mice (N=3), 8–10 weeks old, were obtained from Jackson Laboratories (Bar Harbor, ME). All mice were maintained on low-fluorescence chow (5LJ5, LabDiet, St. Louis, MO) for a minimum of one week prior to initiation of imaging studies. A 300 μl injection of tri-color nanoemulsion (red/green/NIR) was administered via tail vein and mice were euthanized for CFT at 24 h post-injection. As an additional control cohort, uninjected control mice were prepared and embedded in OCT alongside the mice injected with nanoemulsion, using the methods described in Sect. 2.3. Quantification of intestinal fluorescence/auto-fluorescence in the injected and uninjected control mice, respectively, was performed using FIJI software.

Acute Inflammation Model

We employed a model for acute inflammation using carrageenan injected into the hind paw, which has previously been used for *in vivo* ^{19}F MRI, ^{89}Zr PET, and fluorescence imaging using nanoemulsion [10, 16]. Female CD-1 mice (N=3), 8–10 weeks old, were obtained from Envigo (Indianapolis, IN). A 1% λ -carrageenan (Sigma-Aldrich, St. Louis, MO) solution was prepared in saline for subplantar injection (50 μl) into the right hind paw [17]. Paw width and thickness were measured using calipers to confirm swelling due to inflammation. Intravenous di-color nanoemulsion was injected at 24 h post-induction, followed by euthanasia for CFT at 48 h.

Inflammatory Bowel Disease Model

C57BL/6 mice (N=3), 8–10 weeks old, were obtained from Jackson Laboratories. Drinking water was supplemented with 3% dextran sulfate sodium salt (DSS, Spectrum Chemical, New Brunswick, NJ) on Day 0 and offered ad libitum for 10 days to induce acute IBD [18]. Animals were weighed daily and observed for stool consistency and hemocult. Mice in this model were injected with a tri-color nanoemulsion cocktail and euthanized 24 h thereafter for CFT.

Solid Tumor Model

Two different solid tumor models were studied. C57BL/6 mice bearing colon adenocarcinoma MC38 tumors were administered single color nanoemulsion (NIR, 200 μ l) when tumors reached ~1 cm diameter and sacrificed 24 h thereafter. In a second model, murine breast cancer 4T1 cells were implanted into the fourth mammary fat pad of 6–8 week old, female Balb/c mice (N=3, Jackson Laboratory). Tumor volumes were monitored using calipers. A 200 μ l di-color nanoemulsion cocktail was injected at 35 days post implantation, once tumors reached 1,500–2,000 mm³. Mice were sacrificed for CFT 24 h thereafter.

Sample Preparation

Animals were euthanized by CO₂ gas and frozen by submersion in a bath of hexanes in dry ice. A block mold was assembled with squid-ink spaghetti fiducials placed perpendicular to cutting plane for image alignments. The mold was chilled on dry ice, and mice were then embedded for coronal sectioning in OCT compound poured into the chilled mold, followed by storage overnight at -20 °C. Some mice were frozen in an orientation suitable for axial sectioning (Controls and IBD model) in a similar manner as above. The total sample prep time from euthanasia to frozen block is ~12 h, due in large part to the overnight freezing process. Up to ~6 whole mice can be embedded in a single block.

CFT Data Acquisition

For CFT, the frozen block was transferred to the cutting stage inside the cryo-chamber (-15 °C) of the CFT cryostat (Xerra™, Emit Imaging, Baltimore, MD) and the temperature was equilibrated for 2 h. Initial pre-cuts were used to surface the block, and a camera autofocus feature was applied to laboratory pen markings placed on block face. Gain and exposure times were determined automatically and recorded by the instrument on a per-slice basis. The CFT employed a 12 mega-pixel camera with maximum of 4,096 × 3,008 pixel images, capable of resolving isotropic

voxels as small as 20 μ m³ for small fields of view. Whole mice were robotically sectioned at 50 μ m increments, imaging the block face between cuts. Brightfield images were acquired sequentially, followed by laser illumination at 470 nm (green), 555 nm (red), or 730 nm (NIR), with discrete emission filters inserted robotically into light path (511/20 nm for green, 620/14 nm for red, and 794/32 nm for NIR) prior to camera capture. The process of sectioning and imaging is entirely automated. For data acquired using a single fluorescence channel, with 44 μ m² x-y resolution and a 50 μ m slice thickness, a total of ~8 h are required to section and digitize the block.

Image Data Processing

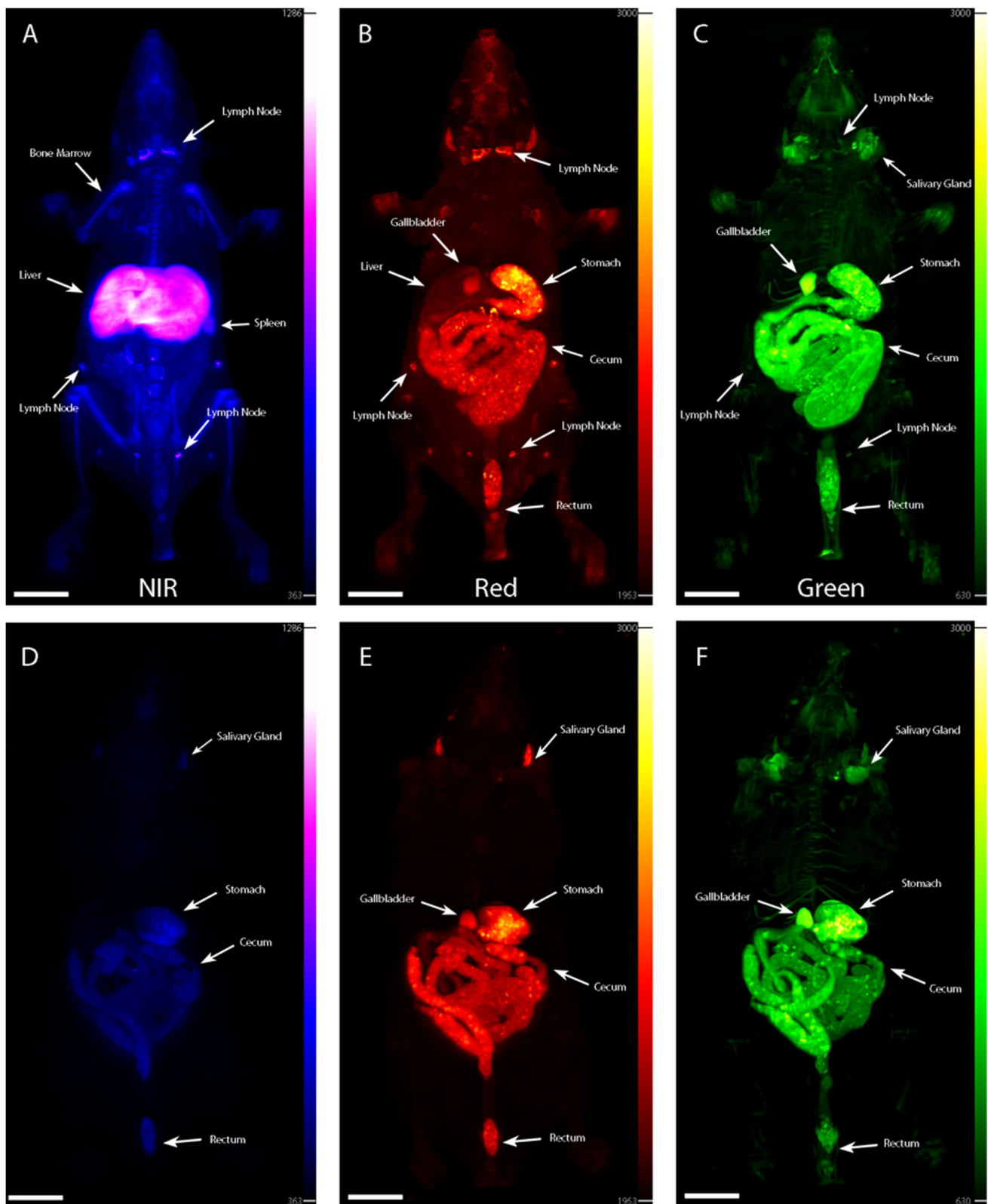
CFT data were initially processed using vendor supplied software (Emit Imaging, Recon Version 1) running on a Dell Precision 7820 with dual 2.3 GHz Intel Xeon Gold 5218 processors and 128 GB random access memory. Within this software, image slices are automatically aligned via reference to the spaghetti fiducials. Regions of interest (ROIs) were selected (e.g., whole-mouse) for image reconstruction using the anatomical information provided by brightfield images as a guide. Subsurface correction and intensity normalization were performed relative to a reference ROI located in a region of OCT devoid of tissue using software-supplied algorithms. Three-dimensional images of each subject were reconstructed and exported as MHD/JPEG image stacks (brightfield) or MHD/RAW and TIFF image stacks (fluorescent images). Images were rendered using VivoQuant (Invivo, Needham Heights, MA.). For maximum image projects (MIPs), a 3 × 3 pixel median filter was applied. Where required, further alignment was performed using FIJI [19].

Results

CFT paired with PFC nanoemulsions are highly effective for visualization of RES compartments and lesion inflammatory infiltrates. Wavelength-dependent autofluorescence and light absorption/scattering may confound probe localization but can also enhance anatomical interpretations.

Wild-Type Control Mice

In wild-type subjects (Fig. 1), PFC nanoemulsions incorporating NIR, red, and green dyes accumulate in RES tissues including the liver, spleen, bone marrow and lymph nodes, as previously observed in ¹⁹F MRI and PET studies [6, 10, 11, 20]. Visible differences are observed in the fluorescence



signals for each channel, attributed to a combination of structural differences between tissues and attenuation of particular wavelengths of incident and emitted light due to

tissue-specific chromophores [21, 22]. Although fluorescence signal from the emulsion is clearly visible with NIR (Fig. 1A) and weakly visible in the red channel (Fig. 1B),

Fig. 1 CFT of wild-type mice showing fluorescent PFC nanoemulsion biodistribution and intrinsic tissue autofluorescence. Shown are maximum intensity projections (MIPs) of NIR (A,D; 730 nm laser, 794/32 filter), red (B,E; 555 nm laser, 620/14 filter), and green (C,F; 470 nm laser, 511/20 filter) channels. In A-C, mouse (C57BL/6) was injected with a triple cocktail of NIR, red, and green PFC nanoemulsion and imaged 24 h thereafter. Panels D-F display MIPs in un-injected mouse exhibiting intrinsic autofluorescence in NIR (D), red (E), and green (F) channels. Reference anatomical structures are labeled. Supplemental data provides 3D MIP animations of Fig. 1 datasets. Scale bars represent 1 cm

signal in the green channel (Fig. 1C) is not observed in blood-rich tissues, specifically the liver and bone marrow, presumably due to interaction of these wavelengths with hemoglobin [23]. Overall, the NIR channel is most representative of the true nanoemulsion biodistribution, resembling signals acquired by ^{19}F MRI [11]. Accumulated populations of labeled phagocytes are visible within the periphery of the lymph nodes for all wavelengths studied, potentially attributable to subcapsular macrophages or follicular dendritic cells.

In control mice without nanoemulsion injection (Figs. 1D-F), autofluorescence is clearly observed in the gall bladder, stomach, and intestines, and can provide vivid anatomical context, particularly in the red and green channels (Fig. 1E,F). Prominent light scattering from fur is also observed in the green channel (Fig. 1F). 3D maximum intensity projection (MIP) animations of Fig. 1 datasets are provided in Supplemental Data.

Axial sections from both un-injected control mice (Figs. 2A-C) and mice injected with PFC nanoemulsion (Figs. 2D-F) imaged in the same block appear similar. Thus, autofluorescence originates primarily from the intestinal contents at all three wavelengths, especially in the lumen of the intestine. In this region green autofluorescence is particularly prominent (Fig. 2C,F), presumably due to collagen and elastin.

Acute Inflammation Model

In the carrageenan model, inflammation is readily visible in the red channel in the injected right paw (inset, Fig. 3D) and in the upper hindlimbs, as well as within lymph nodes throughout the body (Fig. 3A,C). Autofluorescence is visible in the intestinal tract, stomach, and gall bladder. In this model, green signal is only observed throughout the coat, intestines, stomach, and gall bladder, and is not detectable in inflammatory lesions (Fig. 3B,C), possibly due to fluorescence quenching of the green fluorophore.

Inflammatory Bowel Disease Model

The IBD model displays clear NIR signal (Fig. 4A) in the descending colon, due to bowel inflammation, and liver, both of which are consistent with prior studies employing *in vivo* ^{19}F MRI with immunohistochemistry validation [24]. Due to autofluorescence in the intestinal contents, the signal from the red/green nanoemulsion cannot be easily discerned from the background (Fig. 4B,C). Notably, the signal is more clearly localized in the lumen (Fig. 4D-I) in axial and coronal slices. MIPs of autofluorescence are informative, rendering the anatomy clearly visible throughout the gastro-intestinal tract and providing a semi-transparent reference on which to overlay the 3D rendering of the inflammatory lesion. Interestingly, red/green nanoemulsion fluorescence quenching in the liver is readily observed compared to the NIR images (Fig. 4A-C, G-I).

Solid Tumor Models

Mice injected with NIR nanoemulsion show strong signal in the MC38 tumor (Fig. 5A), with minimal signal from intestinal contents. Strong signal is also observed in the liver, spleen, lymph nodes and bone marrow. These observations are consistent with non-invasive ^{19}F MRI and PET TAM imaging studies in different solid tumor models [5, 10, 11, 25].

The red/green nanoemulsion proved less effective at visualizing tumor phagocytes in the 4T1 example (Fig. 5B-D), with autofluorescence from the intestinal contents dominating the red and green channels. When the tumor itself is segmented (bottom panels, Fig. 5B-D), however, high resolution sub-tumoral signals localized in the tumor margin, invasive front, and tumor center are observed in the red/green channels.

Discussion

In this paper we explore the use of fluorescent PFC nanoemulsions for producing high-resolution three dimensional images of probe biodistribution by CFT. Studies were conducted in murine models of acute inflammation, IBD, and solid tumor, all of which demonstrate significant macrophage involvement. Nanometer-sized probes such as PFC nanoemulsions exploit highly evolved cell phagocytic functions for efficient intracellular probe labeling *in situ*. Upon PFC cell labeling, the fluorescent droplets coalesce into lysosomal vesicles and macropinosomes [9], yielding durable labeling without exocytosis for the life of the cell. The biocompatibility and pharmacokinetics of PFC nanoemulsions are well characterized over many decades of research, and the biological inertness and high gas solubility of

liquid-core PFC emulsions have made them candidates for oxygen-carrying blood substitutes [15, 26]. Perfluorocarbons are simultaneously lipophobic and hydrophobic, do not incorporate into cell membranes [14], do not degrade *in vivo* due to enzymes or low pH [14], and clear the body without chemical modification via lung exhalation [27] with a half-life of > 250 days for the nanoemulsion PFC molecule (perfluoropolyether) used in this study.

In situ macrophage labeling with PFC nanoemulsions has been used in a multitude of *in vivo* preclinical imaging studies. For example, ^{19}F MRI studies have been conducted in myocarditis [28], solid organ transplant rejection [29], inflammatory bowel disease (IBD) [24, 30], ischemic stroke [31], acute infection [32], peripheral nerve inflammation [33], multiple sclerosis [6, 20], and TAMs [5, 25, 34] using the same nanoemulsion formulation employed in this study. Importantly, these and other studies provide a histological characterization of the cell phenotypes that take up nanoemulsions, with Ly6C+ monocytes/macrophages comprising the dominant phenotype in lesions yielding detectable signal. *In situ* uptake is ‘pan-macrophage’, analogous to CD68+ immunostaining, with no known uptake specificity among the spectrum of ‘reparative’ and ‘pro-inflammatory’ macrophage subtypes

[35]. Phagocytic neutrophils are also known to take up nanoemulsion, but are physically smaller than macrophages with a ~fourfold lower volume, and thus have less intrinsic ability to take up tracer mass compared to macrophages/monocytes. As a result, their contribution to the observed signal on a per cell basis is significantly lower compared to macrophages. Similarly, lymphocytes will take up trace amounts of agent *in situ*, but provide no significant signal contributions.

Our study suggests that CFT can provide a powerful histological tool for validating putative *in vivo* ‘hot-spot’ signals from PFC nanoemulsions using ^{19}F MRI and PET [10] detection. The CFT method is highly complementary to these *in vivo* imaging techniques, providing near-cellular, sub-tissue localization. For example, in previous studies employing PFC nanoemulsions for visualization of inflammation in a dextran sulfate sodium-induced IBD model using PET and MRI [10], it was difficult to discern whether the tracer was localized in the intestinal lumen or the intestinal contents due to the lack of 3D resolution. The former can be easily confirmed using CFT (Fig. 4).

For applications such as CFT, nanoemulsions are complexed with fluorophores to create ‘dual-mode’ PFC-fluorescent agents for ^{19}F MRI and optical detection.

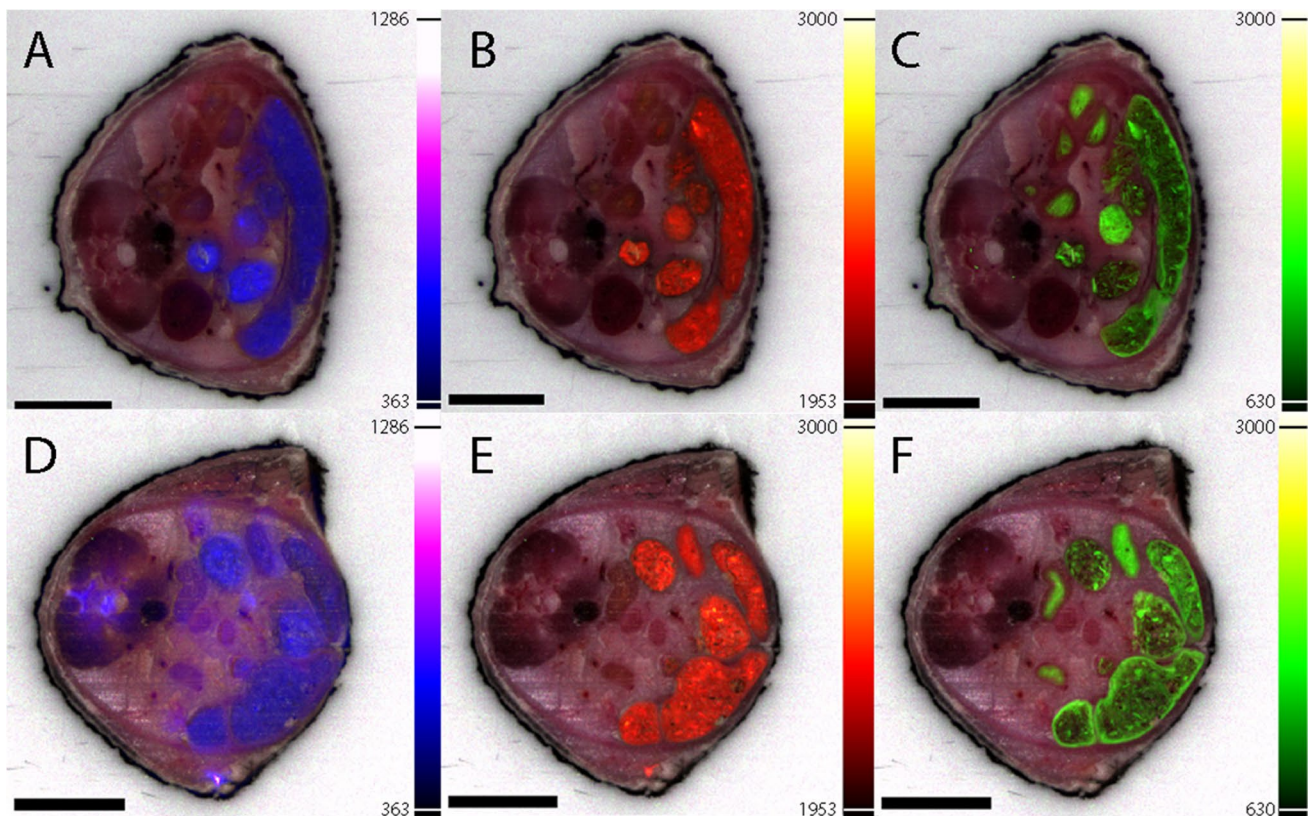


Fig. 2 Axial CFT sections through the intestine of C57BL/6 mouse with no PFC nanoemulsion injected (A–C) and with nanoemulsions injected (D–F). Panels show autofluorescence in lumen (A; 730 nm

laser, 794/32 filter, B; 555 nm laser, 620/14 filter, and C; 470 nm laser, 511/20 filter), and injected and un.injected animals appear similar. Scale bars represent 1 cm

Direct conjugation of dye to fluorophore molecules prior to nanoemulsion formulation ensures that the fluorescent signal's stability remains associated with the nanoemulsion inside PFC labeled cells [12, 36]. Alternatively, a lipophilic fluorescence dye (*e.g.*, $C_{59}H_{97}ClN_2O_4$ or 'DiI') can be incorporated into nanoemulsions formulated with lipid surfactant [6, 9]. Moreover, convenient 'click' chemistry attachment of azide-functionalized fluorophores to the nanoemulsion surfactant has recently been demonstrated [16]. The flexibility of click tracers enables rapid adaptation to suit a wide variety of models and experimental use cases.

Limitations to the interpretation of data generated using fluorescent probes include the presence of tissue autofluorescence, fluorescent light absorbance, and light scattering, each which can give rise to false-positive and false-negative signals [37]. Prominent autofluorescence from endogenous fluorophores is observed in gut and skin [38]. This effect is wavelength dependent, with endogenous fluorophores like chlorophyll, breakdown products, flavins, lipofuscin, collagen and elastin in the intestinal lumen fluorescing in the green channel [39], as clearly observed in Fig. 2C. In the case of gut, chlorophyll autofluorescence can be ameliorated to some extent via specialized diets to reduce fluorescence over the spectral ranges of interest. Gallbladder autofluorescence is also commonly observed, as in Fig. 1, due to presence of bilirubin and biliverdin [40]. Endogenous tissue fluorescence alone is not necessarily detrimental, however, and can have diagnostic value for

the identification of disease pathologies, particularly in the liver [38].

Strategies to discern probe fluorescence signals include use of wavelengths that do not interact significantly with biological tissues and comparison of datasets collected with fluorophores spanning multiple wavelengths [41]. Importantly, a strength of CFT lies in its capacity for multiplex detection of commercially available fluorescent probes thereby permitting flexibility in probe wavelength. To that end, our data confirm that intrinsic autofluorescence may be reduced by utilization of NIR fluorophores within the nanoemulsion, which avoid the spectral range of naturally abundant fluorophores in biological tissues.

Moreover, attenuation of fluorescence signal through scatter of incident or emitted light is a major problem for fluorescence imaging techniques. Absorptive and refractive properties of endogenous biomolecules such as hemoglobin, collagens, and flavins may result in attenuation of incident radiation and emitted fluorescence signals. This is observed in liver and bone marrow, as evident from comparisons of the NIR, red, and green images (Fig. 1). Light scattering off skin surface and fur may also contribute to background fluorescence signals, as observed in the green channel (Fig. 5B).

In current practice, CFT does not have the ability to support whole mouse immunostaining for tracer co-localization studies, nor does the technique have sufficient resolution to resolve individual cells, preventing visual co-localization. Although we have experimented with stopping the

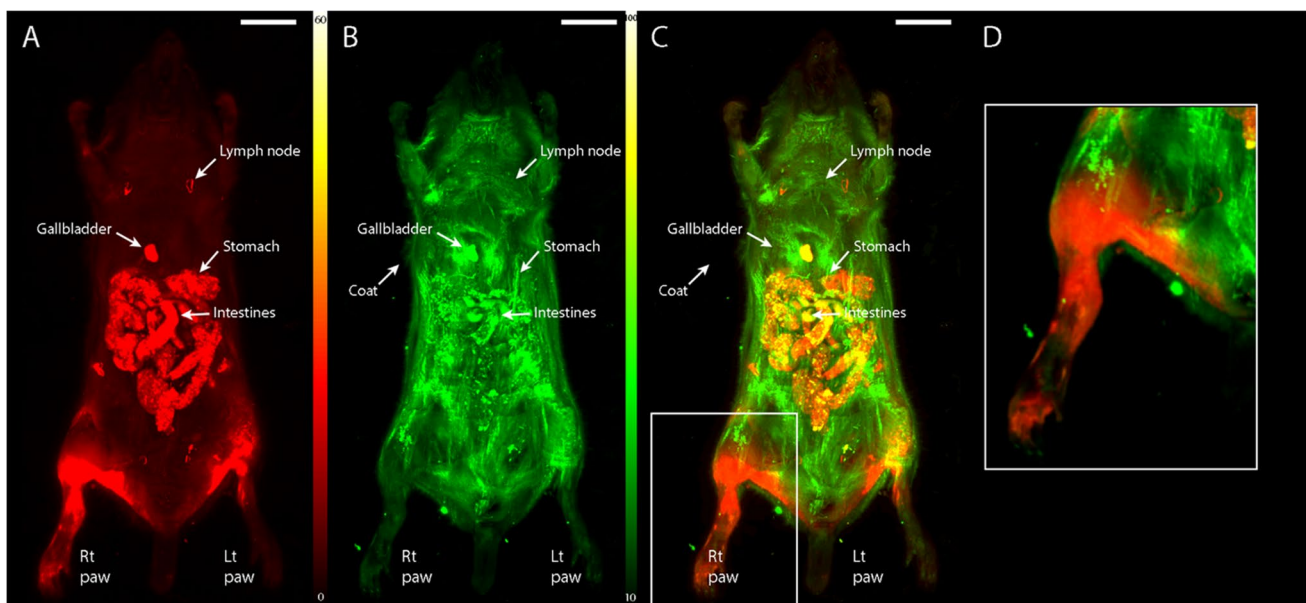


Fig. 3 CFT in acute inflammation model. Carageenan was delivered to right hind paw in CD1 mouse. In (A), inflammation is apparent in right footpad extending into the upper hindlimb in the red channel. Panel (B) displays significant autofluorescence and scattering from

the coat in the green channel, (C) displays an overlay of the red/green channels, and (D) displays a zoomed-in view of inflammation in the right hind paw, boxed in panel (C). Scale bars represent 1 cm

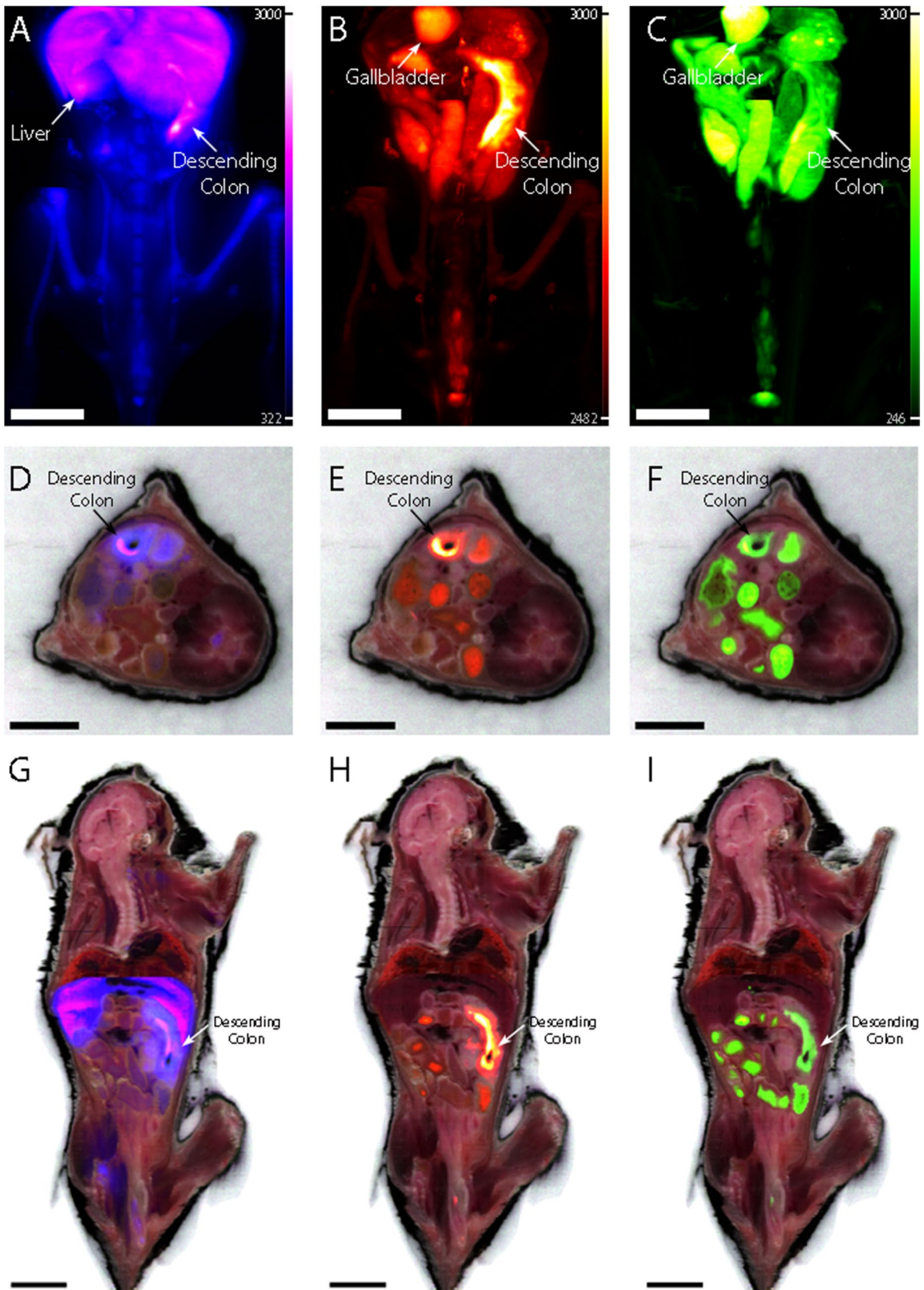


Fig. 4 CFT in IBD mouse model. Shown are MIPS of a C57BL/6 mouse with DSS-induced intestinal inflammation and injected with tricolor PFC nanoemulsion cocktail (**A**; 730 nm laser, 794/32 filter, **B**; 555 nm laser, 620/14 filter, and **C**; 470 nm laser, 511/20 filter). Panels (**D,E,F**) and (**G,H,I**) display axial and coronal sections, respectively, for the same mouse with white light underlay and displays the wall thickening (arrows) in the descending colon, and increased signal compared to the wild-type mouse (Fig. 1). Scale bars represent 1 cm

cryotome mid-sample and transferring a single slice onto histology tape for subsequent histology processing, recovering intact slices in this manner is challenging with current instrumentation.

Currently, this CFT approach is intended for qualitative fluorescence, analogous to widely used *in vivo* fluorescence imaging methods [42]. Quantitative fluorescence imaging of tissues *in situ* is challenged by non-linear signal effects due to dye aggregation and self-quenching inside intracellular vesicles which may reduce bulk tissue fluorescence, as well as the wavelength-dependent impact of the particular tissue's absorbance/scattering properties. Quantitative fluorescence measurements (e.g., dye or nanoemulsion mass) in a tissue region of interest based on CFT data would require a future validation study, perhaps aided by external fluorescence quantification standards. Moreover, algorithmic methods for quantitative comparisons among individual

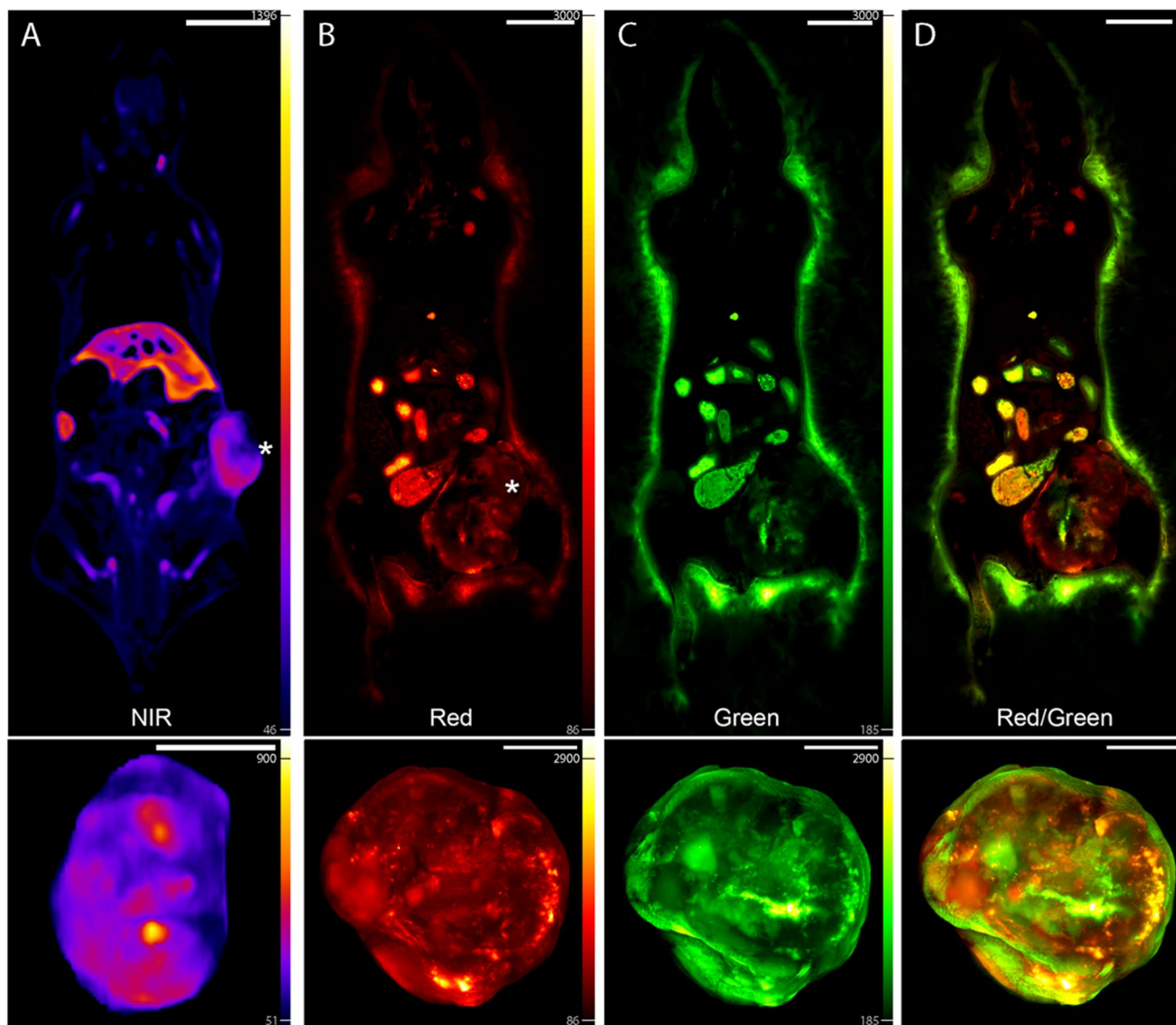


Fig. 5 CFT in solid tumor models. Panels (**A**) display MIPS of MC38 tumor in flank (asterisk) in a mouse injected with NIR PFC nanoemulsion, where the bottom panel shows segmented tumor. In (**B**)–(**D**), MIPS from a mouse with 4T1 flank tumor (asterisk) injected with di-color (red/green) are shown (**B**; 555 nm laser, 620/14 filter,

C; 470 nm laser, 511/20 filter, **D**; overlay), where the lower panels are the segmented tumor. Scale bars represent 1 cm for whole mouse images in the top panels and 0.1 cm for segmented tumor images in the bottom panels

mice, or among cohorts with varying treatments, do not yet exist and would be computationally demanding due to the size of CFT data sets (~ 100 GB/mouse per fluorescence channel). Moreover, by combining CFT data with more quantitative whole-body imaging methods in the same subjects, such as PET [10] or ^{19}F MRI methods that use PFC nanoemulsion tracers (abiet at lower resolution), one could calibrate and benchmark absolute dye mass in fluorescent CFT imagings. A recent study displays the quantitative biodistribution of PFC nanoemulsion in C57BL/6 J mouse using quantitative ^{19}F magnetic resonance spectroscopy [43]; this study reports absolute F-levels and should represent ground-truth values.

Conclusions

Fluorescent PFC nanoemulsions represent a powerful multimodal probe platform for preclinical imaging of inflammation which, in conjunction with CFT, presents a valuable, high-resolution complement to *in vivo* imaging methodologies. In the course of developing new generations of *in vivo* imaging probes, it is essential to validate image specificity, interpretation, and whole-body biodistribution. Current methods, such as conventional histology, are laborious, prone to sampling error, and render it difficult to observe localized concentrations of cells in the context of whole organs and systems. CFT therefore provides a valuable intermediate-resolution technique to bridge the gap between existing *in vivo* imaging techniques and histological micrographs.

Acknowledgements Funding for ETA was provided by the National Institutes of Health (NIH) grant R01-CA269860.

Declarations

Disclosures D.L., P.M. and H.D. are employees of Invicro LLC. The other authors have nothing to disclose.

References

- Ahrens ET, Bulte JWM (2013) Tracking immune cells *in vivo* using magnetic resonance imaging. *Nat Rev Immunol* 13:755–763
- Roy D, Steyer GJ, Gargasha M, Stone ME, Wilson DL (2009) 3D cryo-imaging: a very high-resolution view of the whole mouse. *Anat Rec (Hoboken)* 292:342–351
- Wang C, Adams SR, Ahrens ET (2021) Emergent Fluorous Molecules and Their Uses in Molecular Imaging. *Acc Chem Res* 54:3060–3070
- Steyer GJ, Roy D, Salvado O, Stone ME, Wilson DL (2009) Cryo-imaging of fluorescently-labeled single cells in a mouse. *Proc SPIE Int Soc Opt Eng* 7262:72620W-72620W72628
- Khurana A, Chapelin F, Xu H et al (2018) Visualization of macrophage recruitment in head and neck carcinoma model using fluorine-19 magnetic resonance imaging. *Magn Reson Med* 79:1972–1980
- Zhong J, Narsinh K, Morel PA, Xu H, Ahrens ET (2015) *In vivo* quantification of inflammation in experimental autoimmune encephalomyelitis rats using fluorine-19 magnetic resonance imaging reveals immune cell recruitment outside the nervous system. *PLoS ONE* 10:e0140238
- Ahrens ET, Zhong J (2013) *In vivo* MRI cell tracking using perfluorocarbon probes and fluorine-19 detection. *NMR Biomed* 26:860–871
- Janjic JM, Ahrens ET (2009) Fluorine-containing nanoemulsions for MRI cell tracking. *Wiley Interdiscip Rev Nanomed Nanobiotechnol* 1:492–501
- Ahrens ET, Flores R, Xu H, Morel PA (2005) *In vivo* imaging platform for tracking immunotherapeutic cells. *Nat Biotechnol* 23:983–987
- Wang C, Leach BI, Lister D et al (2021) Metallofluorocarbon nanoemulsion for inflammatory macrophage detection via PET and MRI. *J Nucl Med* 62:1146–1153
- Balducci A, Wen Y, Zhang Y et al (2013) A novel probe for the non-invasive detection of tumor-associated inflammation. *Onco-Immunology* 2:e23034
- Janjic JM, Srinivas M, Kadayakkara DK, Ahrens ET (2008) Self-delivering nanoemulsions for dual fluorine-19 MRI and fluorescence detection. *J Am Chem Soc* 130:2832–2841
- Patrick MJ, Janjic JM, Teng H et al (2013) Intracellular pH measurements using perfluorocarbon nanoemulsions. *J Am Chem Soc* 135:18445–18457
- Krafft MP, Chittofrati A, Riess JG (2003) Emulsions and microemulsions with a fluorocarbon phase. *Curr Opin Colloid Interface Sci* 8:251–258
- Squires JE (2002) Artificial blood. *Science* 295:1002–1005
- Perez AS, Zhou J, Leach B, et al (2021) Click-Ready Perfluorocarbon Nanoemulsion for ^{19}F MRI and Multimodal Cellular Detection. *ACS Nanoscience Au*
- Posadas I, Bucci M, Roviezzo F et al (2004) Carrageenan-induced mouse paw oedema is biphasic, age-weight dependent and displays differential nitric oxide cyclooxygenase-2 expression. *Brit J Pharmacol* 142:331–338
- Okayasu I, Hatakeyama S, Yamada M, Ohkusa T, Inagaki Y, Nakaya R (1990) A novel method in the induction of reliable experimental acute and chronic ulcerative colitis in mice. *Gastroenterology* 98:694–702
- Schindelin J, Arganda-Carreras I, Frise E et al (2012) Fiji: an open-source platform for biological-image analysis. *Nat Methods* 9:676–682
- Ahrens ET, Young W-B, Xu H, Pusateri LK (2011) Rapid quantification of inflammation in tissue samples using perfluorocarbon emulsion and fluorine-19 nuclear magnetic resonance. *Biotechniques* 50:229–234
- Sandell JL, Zhu TC (2011) A review of *in-vivo* optical properties of human tissues and its impact on PDT. *J Biophotonics* 4:773–787
- Jacques SL (2013) Optical properties of biological tissues: a review. *Phys Med Biol* 58:R37–61
- Schaeffter T (2005) Imaging modalities: principles and information content. *Prog Drug Res* 62:15–81
- Kadayakkara DK, Ranganathan S, Young WB, Ahrens ET (2012) Assaying macrophage activity in a murine model of inflammatory bowel disease using fluorine-19 MRI. *Lab Invest* 92:636–645
- Makela AV, Foster PJ (2018) Imaging macrophage distribution and density in mammary tumors and lung metastases using fluorine-19 MRI cell tracking. *Magn Reson Med* 80:1138–1147

26. Geyer RP (1973) Fluorocarbon-polyol artificial blood substitutes. *N Engl J Med* 289:1077–1082
27. Spahn DR (1999) Blood substitutes. Artificial oxygen carriers: perfluorocarbon emulsions. *Crit Care* 3:R93-97
28. Flögel U, Ding Z, Hardung H et al (2008) In vivo monitoring of inflammation after cardiac and cerebral ischemia by fluorine magnetic resonance imaging. *Circulation* 118:140–148
29. Hitchens TK, Ye Q, Eytan DF, Janjic JM, Ahrens ET, Ho C (2011) ¹⁹F MRI detection of acute allograft rejection with in vivo perfluorocarbon labeling of immune cells. *Magn Reson Med* 65:1144–1153
30. Shin SH, Kadayakkara DK, Bulte JW (2017) In vivo ¹⁹F MR imaging cell tracking of inflammatory macrophages and site-specific development of colitis-associated dysplasia. *Radiology* 282:194–201
31. Vindegaard N, Muñoz-Briones C, El Ali HH et al (2017) T-cells and macrophages peak weeks after experimental stroke: Spatial and temporal characteristics. *Neuropathology* 37:407–414
32. Hertlein T, Sturm V, Kircher S et al (2011) Visualization of abscess formation in a murine thigh infection model of staphylococcus aureus by F-19-magnetic resonance imaging (MRI). *PLoS ONE* 6(3):e18246
33. Weise G, Basse-Luesebrink TC, Wessig C, Jakob PM, Stoll G (2011) In vivo imaging of inflammation in the peripheral nervous system by F-19 MRI. *Exp Neurol* 229:494–501
34. Makela AV, Gaudet JM, Foster PJ (2017) Quantifying tumor associated macrophages in breast cancer: a comparison of iron and fluorine-based MRI cell tracking. *Sci Rep* 7:42109
35. Murray PJ, Allen JE, Biswas SK et al (2014) Macrophage activation and polarization: nomenclature and experimental guidelines. *Immunity* 41:14–20
36. Sletten EM, Swager TM (2014) Fluorofluorophores: fluorescent fluorine chemical tools spanning the visible spectrum. *J Am Chem Soc* 136:13574–13577
37. Olson KR, Gao Y, Arif F et al (2017) Fluorescence quenching by metal centered porphyrins and porypyrin enzymes. *Am J Physiol Regul Integr Comp Physiol* 313:R340–R346
38. Croce AC, Ferrigno A, Bottiroli G, Vairetti M (2018) Autofluorescence-based optical biopsy: An effective diagnostic tool in hepatology. *Liver Internat* 38:1160–1174
39. DaCosta RS, Andersson H, Cirocco M, Marcon NE, Wilson BC (2005) Autofluorescence characterisation of isolated whole crypts and primary cultured human epithelial cells from normal, hyperplastic, and adenomatous colonic mucosa. *J Clin Pathol* 58:766–774
40. Croce AC, Ferrigno A, Santin G, Vairetti M, Bottiroli G (2014) Bilirubin: an autofluorescence bile biomarker for liver functionality monitoring. *J Biophotonics* 7:810–817
41. Bottiroli G, Croce AC (2004) Autofluorescence spectroscopy of cells and tissues as a tool for biomedical diagnosis. *Photochem Photobiol Sci* 3:189–210
42. Wolfbeis OS (2015) An overview of nanoparticles commonly used in fluorescent bioimaging. *Chem Soc Rev* 44:4743–4768
43. Ahrens ET, Helfer BM, O'Hanlon CF et al (2023) Method for estimation of apoptotic cell fraction of cytotherapy using in vivo fluorine-19 magnetic resonance: pilot study in a patient with head and neck carcinoma receiving tumor-infiltrating lymphocytes labeled with perfluorocarbon nanoemulsion. *JITC* 11:e007015

Publisher's Note Springer Nature remains neutral with regard to jurisdictional claims in published maps and institutional affiliations.

Springer Nature or its licensor (e.g. a society or other partner) holds exclusive rights to this article under a publishing agreement with the author(s) or other rightsholder(s); author self-archiving of the accepted manuscript version of this article is solely governed by the terms of such publishing agreement and applicable law.